Initial Condition for Fast Model-Based Iterative Reconstruction of Truncated Projection Data

Dong Hye Ye, Somesh Srivastava, Debashish Pal, Jean-Baptiste Thibault, Ken Sauer, and Charles Bouman

***Abstract*—Model-Based Iterative Reconstruction (MBIR) algorithms have gained increasing attentions in clinical studies as they allow significant dose reduction during CT scans while maintaining the diagnostic image quality. Generally, MBIR algorithms take the filtered-back projection (FBP) image as an initial condition for their optimization. The FBP image then has artifacts with truncated projection data, causing slow convergence of MBIR. To reduce the truncation artifacts in the FBP image, we extend the reconstruction region by extrapolating projection data. In addition, we develop an efficient image processing method which reduces the artifacts associated with projection extrapolation. Our experimental results on one phantom and one real abdominal CT scan with truncated projection data show that our processed initial condition significantly improves the convergence speed of MBIR than the conventional FBP image.**

I. Introduction

Model-Based Iterative Reconstruction (MBIR) algorithms have gained attentions for CT reconstruction due to superior signal to noise ratio and image resolution compared with filtered-back projection (FBP) algorithms [1], [2]. MBIR algorithms typically optimize the objective function which incorporates an accurate system model, statistical noise model, and image prior model [3]. Selecting a good initial condition can save time in reconstruction as the initial condition close to the image that the optimization is heading to can reduce the required number of iterations [4]. This is particularly important for MBIR algorithms as high computational time is a major obstacle for their application to clinical practice.

Since it is difficult to obtain a good initial condition without doing any reconstruction, we normally choose a FBP image to start the optimization of MBIR. However, FBP algorithms require that the scanned object is inside the scanning field-of-view (SFOV) during the entire scanning process. Under many scanning conditions, portions of the scanned object can extend beyond the volume measurable by CT detector. For example, when the patient is either very large or is improperly positioned, portions of the patient are often outside the SFOV defined by the CT scanner. If this happens, truncation artifact occurs at the site of truncation in FBP images [5]. In addition, no information can be observed for regions outside the SFOV. The truncation artifact and missing information outside SFOV can significantly slow down the convergence speed of MBIR when FBP images are used as the initial condition. The slow-down could be worse in gradient-based MBIR algorithms for x-ray CT [6], [7]. In these type of algorithms, low-frequency features (such as flat regions) typically tend to converge faster than high-frequency features (such as object-air boundaries).

Although it is possible to redesign a CT system so that the SFOV is increased for FBP algorithms, significant development time and cost are required. Therefore, we use an efficient projection-extrapolation based method to deal with truncated projection data. Among several algorithms proposed in the past [8], [9], we choose a wideview (WV) algorithm [10] which not only reduces truncation artifacts, but also expands the reconstruction region beyond the SFOV defined by the scanner. The WV algorithm assumes that the truncated portion is a partial cylindrical water object. Then, it extrapolates projections by fitting the cylinder to the projection data outside SFOV based on the magnitude and the slope of truncated projection boundary samples.

Even though the WV algorithm can recover the smooth contour of the truncated portion, it is susceptible to background noise associated with projection extrapolation. In addition, the intensity in the truncated region can be incorrect as the truncated portion is assumed to be water. Therefore, we propose an efficient image processing method which can reduce the background noise and correct the intensity in the truncated region in the WV image. We do so by first identifying truncated regions via Otsu's thresholding [11] and then estimating the intensity in the truncated region using non-local mean (NLM) based inpainting [12].

We investigated our algorithm on two datasets. One is an improperly positioned Torso phantom and the other is a real abdominal CT scan with truncated projection data. Results show that the proposed initial condition is very effective in speeding up the convergence speed of MBIR compared with the conventional FBP image.

II. Method

In this section, we describe our image processing method that reduces the artifacts associated projection extrapolation in the WV image. We call our algorithm WV+ as it improves the WV image in terms of initial condition for MBIR. Given a WV image, we first extract a foreground mask via automatic thresholding to remove background noise. In addition, we identify the truncated region from the foreground mask and correct intensities in truncated regions through image inpainting. In following, we explain the procedures in detail.

D. Ye and C. Bouman are with the School of Electrical and Computer Engineering, Purdue University, West Lafayette, IN, 47907.

S. Srivastava, D. Pal, and J.-B. Thibault are with GE Healthcare Technologies, Waukesha, WI, 53188.

K. Sauer is with the Department of Electrical Engineering, University of Notre Dame, IN, 46556.

The authors acknowledge GE Healthcare for supporting this work.

A. Removing Background Noise

Let $x \in \mathbb{R}^N$ be the input WV image which is contaminated by background noise associated with projection extrapolation. In order to remove background noise, we extract the foreground mask via thresholding. Here, the threshold level plays an important role in removing background noise correctly. If the threshold level is too high, parts of anatomy can be recognized as background noise. If the threshold level is too low, background noise will still be present in the initial condition. So, we find the optimal threshold level T which best separates intensity distribution between background noise and interested anatomy.

One may heuristically find T for one scan and use this T for all other CT scans. However, intensity distribution in background noise and interested anatomy can be different across CT scans. Therefore, we should adaptively determine T for different CT scans. Toward this, we use an efficient Otsu's method [11]. Assuming bi-modal intensity distribution, Otsu's method separates the image into two classes (i.e. background and foreground) with the arbitrary threshold level t. We now denote $n_B(t)$ and $n_F(t)$ as the number of pixels in background and foreground, respectively. Then, we calculate the inter-class variance $\sigma^2(t)$ between two classes as following:

$$\sigma^2(t) = n_B(t) \cdot n_F(t) \cdot (\mu_B(t) - \mu_F(t))^2, \tag{1}$$

where $\mu_B(t)$ and $\mu_F(t)$ represent the mean for background and foreground given t, respectively.

Otsu's method then finds the optimal threshold level T that maximizes inter-class variance:

$$T = \arg\max_t \sigma^2(t). \tag{2}$$

It is worth noting that we can efficiently solve this optimization with exhaustive search for the full range of t as the computation of $\sigma^2(t)$ is recursive over t.

The foreground mask $m \in \{0,1\}^N$ is then extracted through thresholding the image x by T:

$$m_i = \begin{cases} 1 & \text{if } x_i > T, \\ 0 & \text{if } x_i \leq T, \end{cases} \tag{3}$$

where subscript i represents the pixel location.

We use the foreground mask m to reduce background noise in x. Since background noise associated projection extrapolation is mostly present outside SFOV, we mask out the background region outside SFOV. Let Ω_{SFOV} be the set of pixel locations inside SFOV. Then, the denoised image $\hat{x} \in \mathbb{R}^N$ is computed as following:

$$\hat{x}_i = \begin{cases} 0 & \text{if } m_i = 0 \text{ and } i \notin \Omega_{SFOV}, \\ x_i & \text{if } m_i = 1 \text{ or } i \in \Omega_{SFOV}. \end{cases} \tag{4}$$

B. Inpainting Truncated Region

Even though we reduce background noise in the WV image, there still be artifacts in the truncated region because projection extrapolation assumes the material of truncated portion to be water. Therefore, if the material density in the truncated anatomy is higher than the water density (i.e. soft tissue), the image will be darker in the truncated region.

Let Ω_{TRUN} be the set of pixel locations in the truncated region. We find Ω_{TRUN} by excluding Ω_{SFOV} from m:

$$\Omega_{TRUN} = \{i : m_i = 1 \text{ and } i \notin \Omega_{SFOV}\}. \tag{5}$$

We then inpaint the pixels in Ω_{TRUN} from the pixels in Ω_{SFOV} through non-local means (NLM) framework [12]. The NLM is a weighted average filter based on similar patches in the search region. The weight w_{ij} between i and j pixels is computed as the following form:

$$w_{ij} = \begin{cases} e^{-\frac{||P_i - P_j||_2^2}{h^2}} & \text{if } j \in \Omega_{SFOV}, \\ 0 & \text{if } j \notin \Omega_{SFOV}, \end{cases} \tag{6}$$

where $||\cdot||_2^2$ is the Euclidean distance and h is a decay coefficient. P_i and P_j represent vectors of intensity values taken from the $p \times p$ patches around i and j, respectively. It is worth noting that we compute the weight only for pixels in SFOV to prevent error propagation from outside SFOV.

We use the weight w_{ij} to correct the pixel values in Ω_{TRUN}. Since the computation w_{ij} for all pixels in the image is time-consuming, we only compute the weight in the small search window. Then, the inpainted image $\tilde{x} \in \mathbb{R}^N$ is calculated from the denoised image $\hat{x}$ as following:

$$\tilde{x}_i = \begin{cases} \frac{\sum_{j \in \mathcal{S}_i} w_{ij} \hat{x}_j}{\sum_{j \in \mathcal{S}_i} w_{ij}} & \text{if } i \in \Omega_{TRUN}, \\ \hat{x}_i & \text{if } i \notin \Omega_{TRUN}, \end{cases} \tag{7}$$

where $\mathcal{S}_i$ represents $S \times S$ square search window around i.

III. Experimental Results

We compare our WV+ image with the conventional FBP and WV image in terms of initial condition for MBIR. The data are acquired from a GE CT750HD scanner with 50cm SFOV. All axial images are reconstructed with size of 512×512 and thickness of $0.625mm$. We use two data sets: a Torso phantom scan of 65 slices and a patient scan of 153 slices. Both datasets are truncated due to improper position and large anatomy. We performed MBIR on a standard 2.0GHz clock rate 8 core Intel processor workstation. The MBIR is parallelized so that each core is responsible for updating a sequence of slices along the z-axis. For our WV+ algorithm, we heuristically set the decay coefficient $h = 10$, the patch size $p = 7$, and the search window size $S = 25$.

Figure 1 shows three different initial conditions for a Torso phantom (top row) and a patient scan (bottom row). Figure 1 (a), (b), (c) represent the initial conditions from FBP, WV, and proposed WV+, respectively. We notice that the FBP initial condition has bright artifacts around truncation site and misses anatomy outside SFOV as illustrated in Figure 1 (a). Compared with FBP, WV removes the bright truncation artifact and recovers the lost anatomy outside SFOV. However, the WV initial condition has the darker region outside SFOV than nearby soft tissue in SFOV as shown in Figure 1 (b). Moreover, WV is susceptible to background noise associated with projection

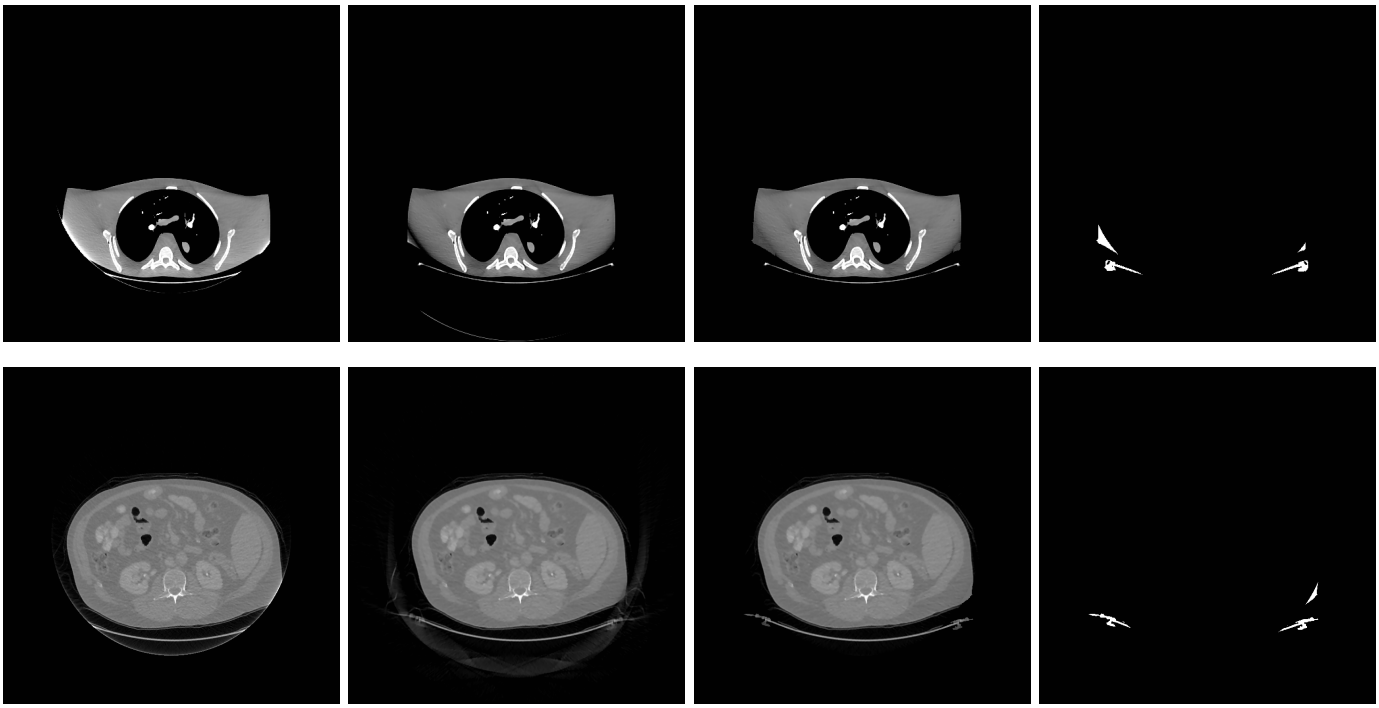

(a) FBP (b) WV (c) WV+ (d) Truncated Region

Fig. 1. Initial conditions for a Torso phantom data (top row) and a patient scan (bottom row): (a) FBP, (b) WV, (c) WV+, (d) Truncated region detected by WV+. The display window of the intensity map is $[700, 1300]$HU for the Torso phantom (top row) and $[0, 2000]$HU for the patient scan (bottom row), respectively. Note that WV+ accurately identifies the truncated region and reduces the artifacts in FBP and WV.

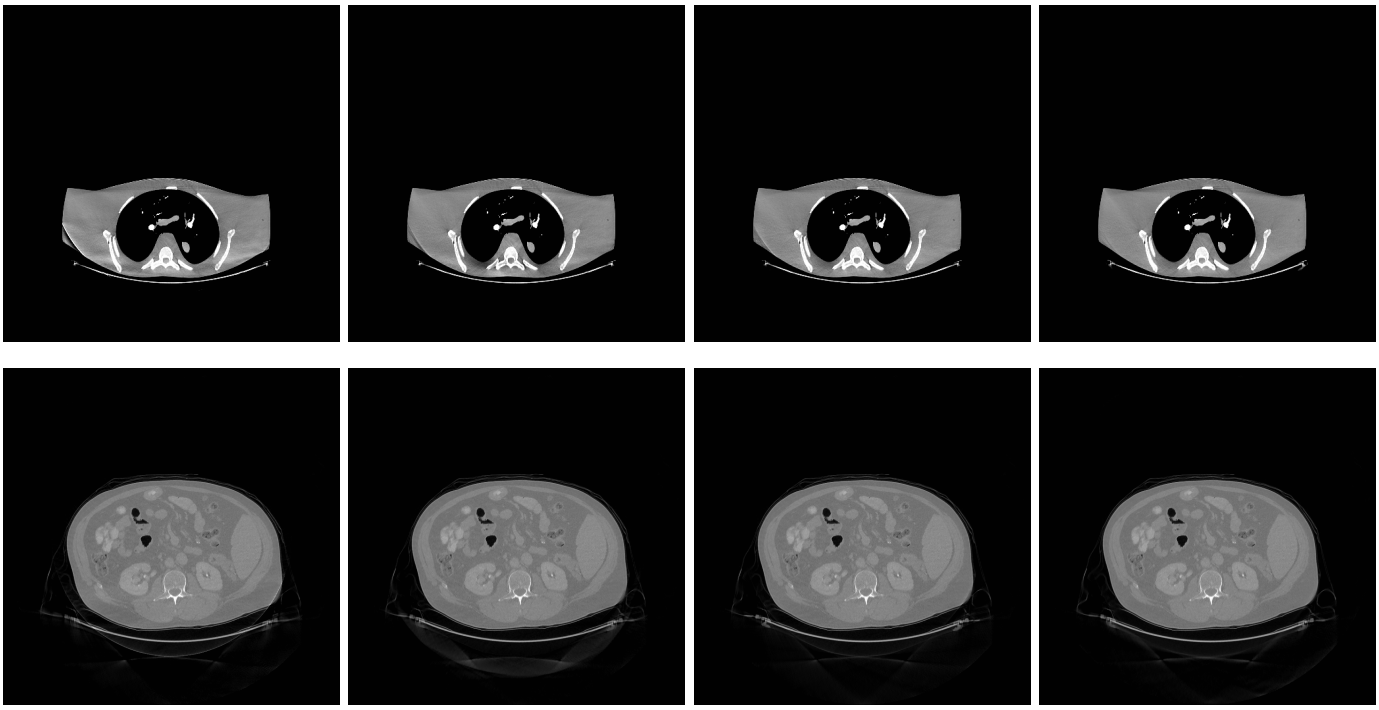

(a) FBP (b) WV (c) WV+ (d) Reference

Fig. 2. Intermediate MBIR results for a Torso phantom data (top row) and a patient scan (bottom row) after 5 iterations: (a) FBP, (b) WV, (c) WV+, (d) Fully-converged reference image after 20 iterations. The display window of the intensity map is $[700, 1300]$HU for the Torso phantom (top row) and $[0, 2000]$HU for the patient scan (bottom row), respectively. Note that WV+ produces closer image to the reference image compared with FBP and WV, reflecting the faster convergence using WV+ as initial condition.

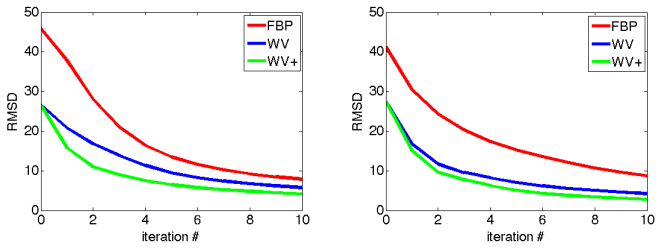

(a) Torso phantom (b) Patient scan

Fig. 3. Root mean square difference (RMSD) between intermediate MBIR results and the fully-converged reference image for 10 iterations: (a) Torso phantom, (b) Patient scan. Red, blue, and green line represent the RMSD plot using FBP, WV, and WV+ initial conditions, respectively. For both cases, WV+ achieves the improvement in convergence speed compared with FBP and WV.

extrapolation. In Figure 1 (c), WV+ corrects the low intensity values in the truncated region and reduces background noise in the WV image. This reflects that automatic thresholding in our WV+ algorithm accurately identifies the truncated region (see Figure 1 (d)) and corrects the dark pixels in the truncated region through NLM based image inpainting.

Figure 2 shows the intermediate MBIR results after 5 iterations for a Torso phantom (top row) and a patient scan (bottom row). Figure 2 (a), (b), (c) represent the intermediate MBIR results using FBP, WV, and proposed WV+ for initial condition, respectively. For reference, we also display the fully-converged MBIR reconstruction after 20 iterations in Figure 2 (d). Using the FBP initial condition, the MBIR results show peripheral ring and bright artifacts in SFOV. In addition, truncated regions are not fully reconstructed as shown in Figure 2 (a). This indicates that the image is under-converged after 5 iterations. Using the WV initial condition, reconstruction result is closer to the fully converged reference image than using FBP as illustrated in Figure 2 (b). But, there exist shading artifacts around lung boundary for a Torso phantom and background noise in a patient scan, reflecting that the reconstruction is not converged yet. With our WV+ initial condition, MBIR generates very close image (see Figure 2 (c)) to the fully converged reference image (see Figure 2 (d)) after 5 iterations. This shows that our WV+ improves the convergence speed of MBIR compared with FBP and WV.

For quantitative comparisons, Figure 3 plots the root mean square difference (RMSD) between intermediate MBIR results and the fully-converged reference image over 10 iterations. We show RMSD trends for the Torso phantom in Figure 3 (a) and for the patient scan in Figure 3 (b). Red, blue, and green curves represent RMSD for FBP, WV, and WV+ initial conditions, respectively. Notice that the FBP initial condition has very slow convergence as 10 iterations are not enough for MRIR to be converged. This is because truncation artifacts and missing anatomy in the FBP image make the initial condition far from the image that the optimization is heading to. By using the WV initial condition, we can achieve much faster convergence than using the FBP initial condition since WV reduces truncation artifacts and recovers missing anatomy in the FBP image. WV+ further improves the convergence speed, showing the benefit of our image processing on the WV image. It is worth noting that the speedup by WV+ compared with WV is larger for the Torso phantom than for the patient scan. This is because the patient scan has less level of truncation and therefore the WV artifacts associated with projection extrapolation are reduced.

IV. Conclusions

In this paper, we present an image processing method to generate the initial condition for MBIR that can improve the convergence speed. Our method is based on projection-extrapolation WV algorithm which reduces truncation artifacts and recovers the lost anatomy in the FBP image with truncated projection data. We further improve the WV by reducing background noise via automatic thresholding and correcting the truncated region via NLM inpainting. Results on both phantom and real datasets show that the proposed algorithm is very effective in improving the convergence speed of MBIR compared with using FBP and WV as initial condition.

References

[1] J.-B. Thibault, K. D. Sauer, C. A. Bouman, and J. Hsieh, "A three-dimensional statistical approach to improved image quality for multislice helical CT," *Medical Physics*, vol. 34, no. 11, pp. 4526–4544, Nov. 2007.

[2] Z. Yu, J.-B. Thibault, C. A. Bouman, K. D. Sauer, and J. Hsieh, "Fast model-based X-ray CT reconstruction using spatially nonhomogenenous ICD optimization," *IEEE Trans. Image Process.*, vol. 20, no. 1, pp. 161–175, Jan. 2011.

[3] J. Hsieh, *Computed Tomograhpy: Principles, Design, Artifacts, and Recent Advances*, 2nd ed. Wiley, 2009, ch. 7, pp. 270–279.

[4] T.-S. Pan, B. Tsui, and C. L. Byrne, "Choice of initial conditions in the ML reconstruction of fan-beam transmission with truncated projection data," *IEEE Trans. Med. Imag.*, vol. 16, no. 4, pp. 426–438, Aug. 1997.

[5] B. Ohnesorge, T. Flohr, K. Schwarz, J. P. Heiken, and K. T. Bae, "Efficient correction for CT image artifacts caused by objects extending outside the scan field of view," *Medical Physics*, vol. 27, no. 1, pp. 39–46, Jan. 2000.

[6] L. Fu, Z. Yu, J.-B. Thibault, B. De Man, M. G. McGaffin, and J. A. Fessler, "Space-variant channelized preconditioner design for 3D iterative ct reconstruction," in *Int'l. Mtg. on Fully 3D Image Recon. in Rad. and Nuc. Med*, Jun. 2013, pp. 205–208.

[7] D. Kim and J. A. Fessler, "Optimized momentum steps for accelerating x-ray ct ordered subsets image reconstruction," in *Int'l. Conf. on Image Formation in X-ray CT*, Jun. 2014, pp. 103–106.

[8] H. R. Hooper and B. G. Fallone, "Technical note: Sinogram merging to compensate for truncation of projection data in tomotherapy imaging," *Medical Physics*, vol. 29, no. 11, pp. 2548–2551, Nov. 2002.

[9] K. J. Ruchala, G. H. Olivera, J. M. Kapatoes, P. J. Reckwerdt, and T. R. Mackie, "Method for improving limited field-of-view radiotherapy reconstructions using imperfect a priori images," *Medical Physics*, vol. 29, no. 11, pp. 2590–2605, Nov. 2002.

[10] J. Hsieh, E. Chao, J.-B. Thibault, B. Grekowicz, A. Horst, S. McOlash, and T. J. Myers, "A novel reconstruction algorithm to extend the ct scan field-of-view," *Medical Physics*, vol. 31, no. 9, pp. 2385–2391, Aug. 2004.

[11] N. Otsu, "A threshold selection method from gray level histograms," *IEEE Trans. Syst. Man Cybern.*, vol. SMC, no. 1, pp. 62–66, Jan. 1979.

[12] A. Wong and J. Orchard, "A nonlocal-means approach to exemplar-based inpainting," in *IEEE Int'l. Conf. Image Proc.*, Oct. 2008, pp. 2600–2603.